nature physics

Article

https://doi.org/10.1038/s41567-023-02144-x

Josephson diode effect derived from short-range coherent coupling

Received: 6 September 2022

Accepted: 23 June 2023

Published online: 31 July 2023

Check for updates

Sadashige Matsuo[1] ✉, Takaya Imoto[1,2], Tomohiro Yokoyama[3], Yosuke Sato[1], Tyler Lindemann[4,5], Sergei Gronin[4], Geoffrey C. Gardner[4], Michael J. Manfra[4,5,6,7] & Seigo Tarucha[1,8] ✉

Typical superconducting materials have both time-reversal symmetry and inversion symmetry. Devices that break these symmetries are expected to have exotic phenomena such as the superconducting diode effect, which can provide lossless rectification. Here, we present a device comprising one Josephson junction coupled to another that exhibits the superconducting diode effect. We show that the observed effect can be controlled non-locally based on the phase difference of the adjacent junction. These results indicate that the time-reversal and spatial-inversion symmetries of a Josephson junction are broken by the coherent coupling to an adjacent junction, and this enables the engineering of superconducting phenomena mediated by interaction among Josephson junctions.

Symmetry breaking in superconducting (SC) devices has led to the emergence of exotic phenomena; for example, Majorana zero modes in SC devices with broken time-reversal and spatial-inversion symmetries have recently been proposed, and possible experimental signatures have been reported[1]. This implies that analysis and control of the symmetry-breaking mechanism in SC devices are crucial not only for understanding such exotic SC phenomena but also for providing flexibility in their engineering design.

The superconducting diode effect (SDE), which is the direction-dependent switching current, namely, the nonreciprocal SC transport, is a characteristic phenomenon occasionally found in SC devices with both time-reversal and spatial-inversion symmetries broken. Nonreciprocal transport can be employed for the rectification of electrical currents represented by p–n junctions. Therefore, dissipationless rectification can be achieved based on the SDE. Several mechanisms for the SDE have been reported in Josephson junction (JJ) devices[2–11], for example, in asymmetric SC quantum interference devices (SQUIDs), where the time-reversal and spatial-inversion symmetries are broken by the induced phase difference and two asymmetric JJs, respectively[12,13,14]. The SDE has also been observed in non-centrosymmetric bulk SC materials under external magnetic fields and even zero magnetic field[15–20].

In this study, we focus on two JJs with short-range coherent coupling[21–24]. This short-range coherent coupling is defined as hybridization of the Andreev bound states in the respective JJs through the shared SC electrode, as described schematically in Fig. 1a. In this device, the time-reversal symmetry can be broken by the induced phase differences, and the spatial-inversion symmetry can be broken by asymmetrically tuning the phase differences of two JJs. The symmetry breaking in the short-range coupled JJs provides important insights for bottom-up engineering of exotic SC phenomena in JJ arrays[25]. Experimental observation of the SDE can elucidate the physics of symmetry breaking in coupled JJs and thus contributes to engineering of exotic SC phenomena. Furthermore, unlike the SDE studied thus far, the SDE in the two coupled JJs can be controlled non-locally by tuning the non-local phase difference. This provides new designability and functionality for the SC circuit applications.

There are reports of nonreciprocal SC transport or SDE measured with two or more current sources[26–31] or a single current source with applied magnetic field[32] in multiterminal JJs, which have more than three SC electrodes in contact with the same single normal metal. Compared to the multiterminal JJ structures in the literature, our coupled JJ structure utilizes overlapping of the Andreev bound state

[1]Center for Emergent Matter Science, RIKEN, Saitama, Japan. [2]Department of Applied Physics, Tokyo University of Science, Tokyo, Japan. [3]Department of Materials Engineering Science, Graduate School of Engineering Science, Osaka University, Osaka, Japan. [4]Birck Nanotechnology Center, Purdue University, Indiana, IN, USA. [5]Department of Physics and Astronomy, Purdue University, Indiana, IN, USA. [6]School of Materials Engineering, Purdue University, Indiana, IN, USA. [7]Elmore Family School of Electrical and Computer Engineering, Purdue University, Indiana, IN, USA. [8]RIKEN Center for Quantum Computing, RIKEN, Saitama, Japan. ✉e-mail: sadashige.matsuo@riken.jp; tarucha@riken.jp

https://doi.org/10.1038/s41567-023-02144-x

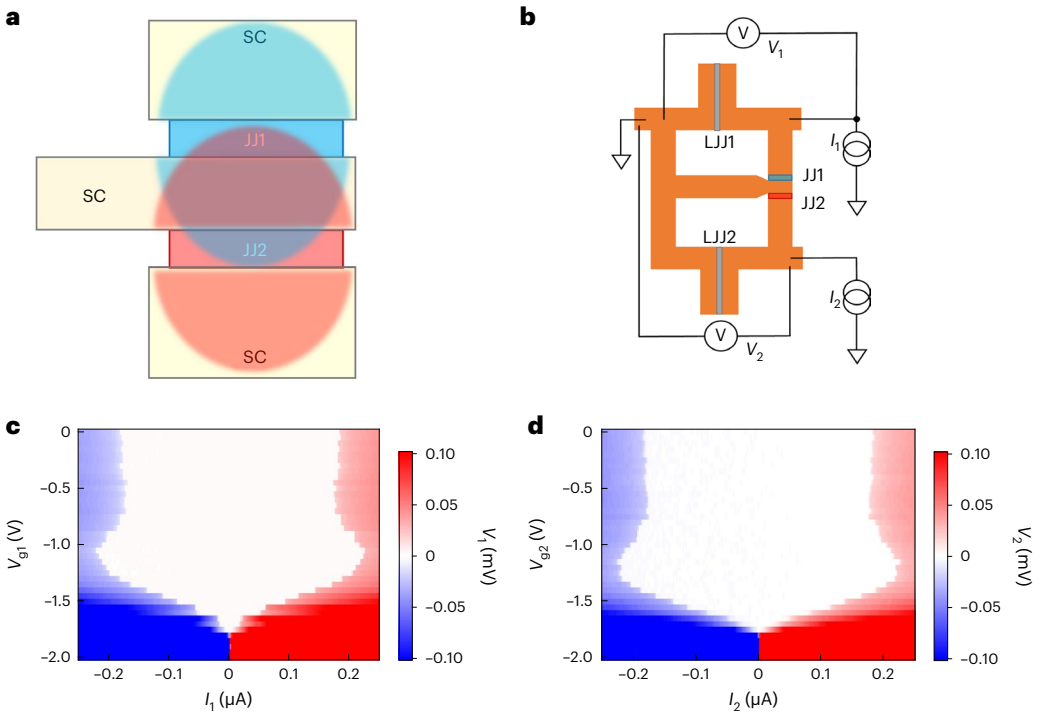

Fig. 1 | Device concept and coherent coupling of JJs. a, A conceptual image of the coherent coupling of two JJs (JJ1 and JJ2). The wavefunctions of the Andreev bound states in the respective JJs penetrate the SC electrodes. When the centre electrode is sufficiently thin to allow the wavefunctions to tunnel into the adjacent JJ, the bound states in the JJs hybridize, resulting in coherent coupling. **b**, A schematic image of our device and measurement setup. Two JJs (JJ1 and JJ2) are fabricated from an InAs quantum well covered by an epitaxial Al film. Additionally, two larger JJs (LJJ1 and LJJ2) are fabricated. When acquiring the data, LJJ1 is always pinched off. Then only JJ2 is embedded in the SC loop with LJJ2, which enables control of the phase difference of JJ2 by an out-of-plane magnetic field. The voltage difference V_1 on JJ1 is measured based on the bias current I_1. **c**, V_1 on JJ1 with JJ2, LJJ1 and LJJ2 pinched off as a function of I_1 and V_{g1} at $B = 0$ mT. The supercurrent disappears at $V_{g1} \cong -1.8$ V. **d**, V_2 on JJ2 with JJ1, LJJ1 and LJJ2 pinched off as a function of the bias current I_2 and V_{g2} at $B = 0$ mT.

wavefunctions through the SC electrode shared by two JJs (Fig. 1a); in this structure, the coherent coupling effect on the SDE is clearly distinguishable and therefore provides evidence of coherent coupling generating the SDE. Coherent coupling might also exist in the multiterminal JJ devices[32]; however, in those devices, the coherent coupling contribution to the SDE cannot be distinguished because an electrical circuit of JJs equivalent to the multiterminal JJs can produce the SDE[30,32], even with no coherent coupling. Furthermore, the coupled JJ structure allows the coherent coupling of various kinds of JJs. This capability will lead to the generation of novel SC phenomena in combinations of various JJs, which cannot be realized in a multiterminal JJ structure. Hence, our study of the fundamental physics of symmetry breaking in the coupled JJs, enabled by measuring the SDE, is of significance.

In this work, we report observation of the SDE in a JJ coupled to an adjacent JJ without Zeeman splitting or use of ferromagnetic materials. The SDE is realized only by control of the non-local phase difference and systematically appears when non-local phase difference is near π. A single current source is used for the observation, which is different from previous reports of multiterminal JJs in which more than two current sources have been used (Supplementary Note 9 and Supplementary Fig. 14). The structure enables measurement of the SDE when the two different JJs realized by gating are coupled. Thanks to this property, analysis of the local and non-local gate-voltage dependencies shows the SDE is enhanced when the two JJs become nearly equivalent. We attribute the origin of the SDE to asymmetric current phase relations (CPRs) resulting from the short-range coherent coupling. Our results demonstrate that coherent coupling of JJs is available for the design of lossless rectifiers in SC circuits and imply that the coupled JJs are availble to realize exotic SC phenomena with the time-reversal and spatial-inversion symmetries broken.

Device characteristics

Physical description

In our experiments, a high-quality InAs quantum well covered by an epitaxial aluminium (Al) thin film was used to form superconductor–semiconductor junctions[33]. This system provides a suitable platform for studying the SC proximity effect in the semiconductor owing to the highly transparent interface between the Al film and the InAs quantum well[34,35].

This quantum well wafer was processed to fabricate a device with two coupled JJs (JJ1 and JJ2). JJ1 and JJ2 are embedded in different SC loops with the LJJ1 and LJJ2, which are sufficiently larger than JJ1 and JJ2, respectively. A diagram of the device is shown in Fig. 1b. All JJs are gate-tunable using voltages to pinch off the junctions. JJ1 and JJ2 have the same structure (junction length and width are 100 nm and 600 nm, respectively) and the distance between them is 150 nm. This distance is much shorter than the coherence length of Al (approximately 1 μm). LJJ1 and LJJ2 are 2 μm wide and 100 nm long (see Supplementary Note 1 and Supplementary Fig. 1 for additional details). When obtaining the results discussed in the main text, LJJ1 was always pinched off. Therefore, the device can be regarded as JJ1 with no loop and JJ2 embedded in the SC loop with LJJ2. An out-of-plane magnetic field was used to control the phase difference of JJ2. Electron transport measurements were performed at a base temperature of 10 mK, achieved by using a dilution refrigerator. We measured JJ1 by sweeping a bias current I_1 to detect a voltage difference V_1, as shown in Fig. 1b. This setup differs from that for the conventional SQUIDs, in which two JJs are embedded in the SC loop. In conventional SQUID measurements, the voltage difference of the two JJs is detected, whereas in our case, JJ1 is outside of the SC loop, and almost all the bias current flows into the centre SC electrode shared by JJ1 and JJ2. This means that the voltage differences

https://doi.org/10.1038/s41567-023-02144-x

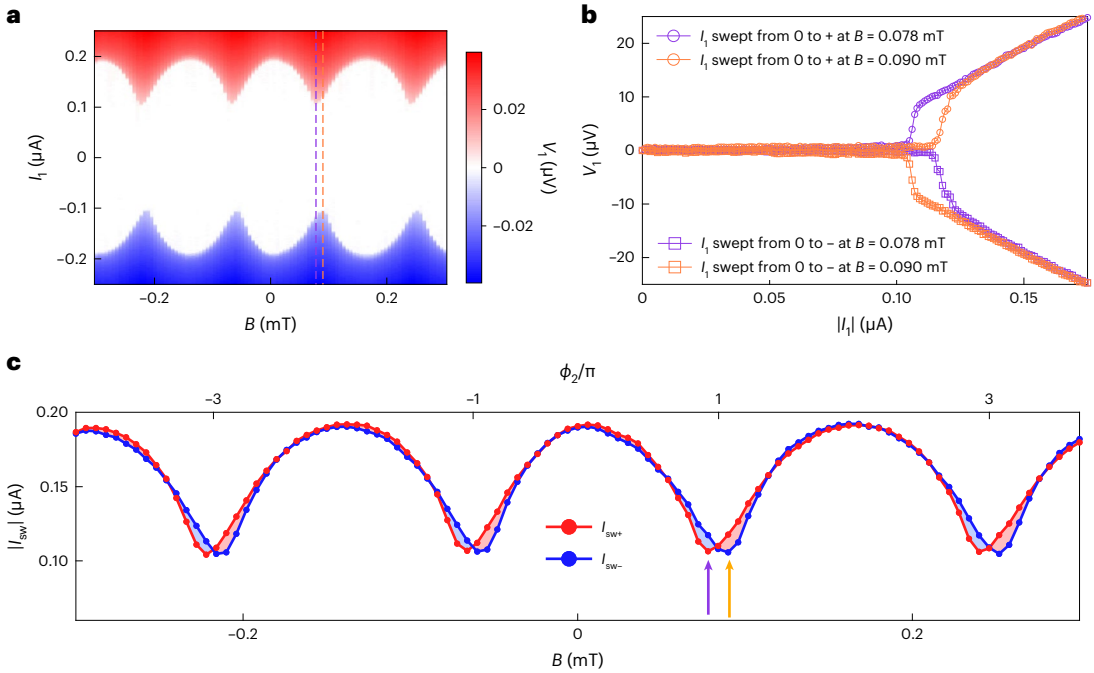

Fig. 2 | Observed SDE. a, V_1 as a function of I_1 and B with $V_{g1} = 0$ V, $V_{g2} = 0$ V, LJJ1 off and LJJ2 on. The oscillation derived from the coherent coupling of JJ1 and JJ2 is observed. The purple and orange dashed lines indicate $B = 0.078$ and 0.090 mT, respectively. **b**, V_1 as a function of $|I_1|$ at $B = 0.078$ and 0.090 mT is indicated by the purple and orange curves, respectively. The circles and squares are obtained as I_1 is swept from 0 to the positive and negative current limits, respectively. The results show that the absolute value of the switching current in the positive direction differs from that in the negative direction, indicating SDE. **c**, $|I_{sw+}|$ and $|I_{sw-}|$ with respect to B represented by the red and blue circles, respectively, indicating that the SDE occurs systematically. In addition, the sign of the SDE is controlled by B (the blue and red shadows highlight regions of $|I_{sw+}| < |I_{sw-}|$ and $|I_{sw+}| > |I_{sw-}|$, respectively). The purple and orange arrows indicate $B = 0.078$ mT and 0.090 mT, respectively.

of JJ2 and LJJ2 are always zero (Supplementary Note 5 and Supplementary Figs. 7–9).

Supercurrent analysis

Gate-voltage dependencies of the single JJs are examined to verify that the supercurrent flows in the JJs through the InAs quantum well. Figure 1c shows V_1 as a function of I_1 and gate voltage V_{g1} for the single JJ1 with JJ2, LJJ1 and LJJ2 pinched off. The supercurrent region where $V_1 \approx 0$ mV disappears at approximately $V_{g1} = -1.8$ V. Similarly, the gate-voltage dependence for the single JJ2 is depicted in Fig. 1d. A negative V_{g2} can suppress the supercurrent through JJ2. These results indicate that the gate voltages on the respective JJs can control the supercurrent flow in the InAs quantum well.

We examined the switching current oscillation of JJ1 coupled to JJ2 embedded in the SC loop. In the device, the supercurrent of JJ1 depends not only on the phase difference of JJ1 but also on the phase difference of JJ2 due to the coherent coupling between the Andreev bound states of two JJs[21]. Hence, the switching current is expected to oscillate as a function of the magnetic field B because the phase difference of JJ2 is controlled by the magnetic flux in the loop[24]. We have measured this oscillation in our device with $V_{g1} = 0$ V, $V_{g2} = 0$ V, LJJ1 off and LJJ2 on. LJJ2 has a switching current sufficiently larger than that of JJ2, and then B controls the JJ2 phase difference with the ignorable change of the LJJ2 phase difference (Supplementary Note 1). Figure 2a shows V_1 as a function of I_1 and B. The white region ($V_1 \cong 0$ mV) indicates supercurrent flow in JJ1. The boundary between the white and red regions defines I_{sw+}, which is the switching current in the positive-current region. Similarly, I_{sw-} (the switching current in the negative-current region) is defined as the boundary between the white and blue regions. Both I_{sw+} and I_{sw-} oscillate as a function of B, as expected from the coherent coupling between JJ1 and JJ2. The oscillation period is 0.156 mT, which is consistent with the calculated period of 0.176 mT for a loop area of 11.7 μm^2. We note that coherence is necessary to obtain these oscillations and then the oscillation disappears in the device with 1 μm separation of JJ1 and JJ2 (Supplementary Note 8 and Supplementary Fig. 13).

To verify the SDE, V_1 versus $|I_1|$ at $B = 0.078$ mT and 0.090 mT is plotted by the purple and orange lines, respectively, in Fig. 2b. The circles and squares represent the data obtained as I_1 is swept from zero to positive and negative limits, respectively. At $B = 0.078$ mT, $|I_{sw+}| = 106$ nA (evaluated from the purple circles) is smaller than $|I_{sw-}| = 116$ nA (evaluated from the purple squares). Conversely, at $B = 0.090$ mT, $|I_{sw+}| = 117$ nA > $|I_{sw-}| = 105$ nA. These results confirm that the SDE occurs in JJ1 and the sign of SDE, namely, the sign of $I_{sw+} + I_{sw-}$, depends on B (Supplementary Note 2 and Supplementary Fig. 2).

To investigate the B-dependence of the SDE, the absolute values of I_{sw+} and I_{sw-} are plotted as a function of B in Fig. 2c, where the red and blue circles represent I_{sw+} and I_{sw-}, respectively. For clarity, the regions where $|I_{sw+}| > |I_{sw-}|$ are coloured in red and those where $|I_{sw+}| < |I_{sw-}|$ are indicated in blue. The SDE ($|I_{sw+}| \neq |I_{sw-}|$) systematically appears in the vicinity of the minimal $|I_{sw}|$ points. This implies that the SDE sign can be easily switched by a change in B. Because of the time-reversal relation of the supercurrent in JJ1, I_{sc1} of the supercurrent in JJ1 should satisfy $I_{sc1}(\phi_1, \phi_2) = -I_{sc1}(-\phi_1, -\phi_2)$, which results in $I_{sc1}(\phi_1, 0) = -I_{sc1}(-\phi_1, 0)$ and $I_{sc1}(\phi_1, \pi) = -I_{sc1}(-\phi_1, \pi)$. Here, ϕ_1 and ϕ_2 are the phase differences of JJ1 and JJ2, respectively. Therefore, we can set $\phi_2 (\mathrm{mod}\ 2\pi) = 0$ and π as crossing points of $|I_{sw+}(B)|$ and $|I_{sw-}(B)|$, as indicated by the top axis in Fig. 2c. It is significant that the condition $I_{sc1}(\phi_1, \phi_2) = -I_{sc1}(-\phi_1, \phi_2)$ is not necessarily satisfied when $\phi_2 (\mathrm{mod}\ 2\pi) \neq 0, \pi$, which allows the emergence of the SDE. Notably, a device with a mirrored structure produces an SDE with the opposite sign (Supplementary Note 3 and Supplementary Fig. 3). The observed SDE features can be experimentally reproduced in a different

https://doi.org/10.1038/s41567-023-02144-x

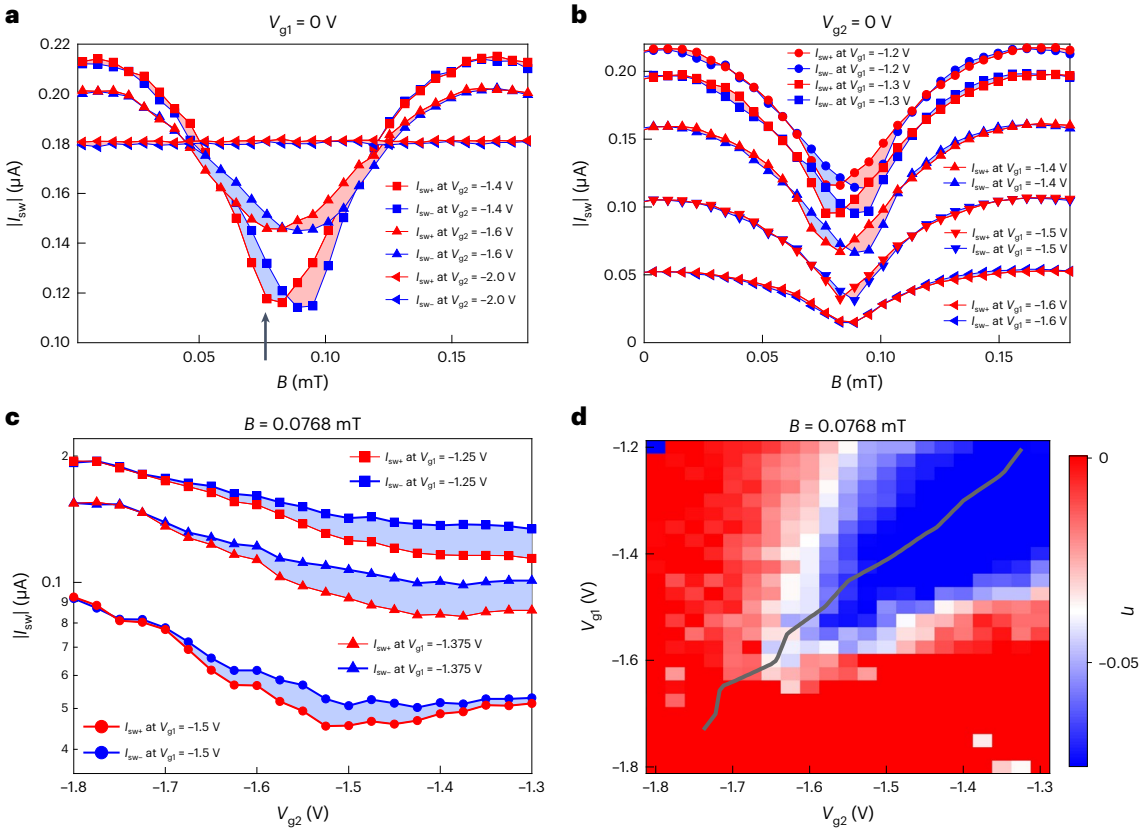

Fig. 3 | Symmetric conditions of JJ1 and JJ2 that generate the SDE. a, $|I_{sw+}|$ and $|I_{sw-}|$ as a function of B at V_{g2} = −1.4, −1.6 and −2.0 V with V_{g1} = 0 V, LJJ1 off and LJJ2 on. The SDE of JJ1 is non-locally controlled by tuning JJ2 with V_{g2} and disappears, as does the oscillation for $V_{g2} \leq -1.8$ V because the supercurrent in JJ2 disappears. The black arrow indicates B = 0.0768 mT. The blue and red shadows highlight regions of $|I_{sw+}| < |I_{sw-}|$ and $|I_{sw+}| > |I_{sw-}|$, respectively. **b**, $|I_{sw+}|$ and $|I_{sw-}|$ as a function of B for V_{g1} = −1.2 to −1.6 V with V_{g2} = 0 V, LJJ1 off and LJJ2 on. When JJ1 is locally controlled with V_{g1}, the SDE decreases as V_{g1} decreases. **c**, $|I_{sw+}|$ and $|I_{sw-}|$ as a function of V_{g2} at V_{g1} = −1.25, −1.375 and −1.5 V with LJJ1 off and LJJ2 on when B = 0.0768 mT. At V_{g1} = −1.25 and −1.375 V, the SDE monotonically decreases as V_{g2} decreases. On the other hand, at V_{g1} = −1.5 V, the SDE becomes maximum at V_{g2} = −1.525 V. **d**, The evaluated η as a function of V_{g1} and V_{g2} at B = 0.0768 mT. The blue region represents when the SDE is enhanced, which is shaped diagonally. The grey curve indicates the gate conditions when single JJ1 and single JJ2 have the same switching currents. The blue SDE region follows the grey curve; this implies that the symmetric condition of JJ1 and JJ2 favours a larger SDE.

device (Supplementary Note 7 and Supplementary Figs. 11 and 12) and also by numerical calculations based on the tight-binding model (Supplementary Note 6 and Supplementary Fig. 10).

Gate-voltage effects on SDE

We studied the gate-voltage dependencies of the SDE to support the assertion that the SDE originates from the coherent coupling, by excluding other mechanisms. Figure 3a presents $|I_{sw+}|$ and $|I_{sw-}|$ as a function of B at V_{g2} = −1.4, −1.6 and −2.0 V with V_{g1} = 0 V, LJJ1 off and LJJ2 on, corresponding to the non-local gate control of JJ1 through the coherent coupling. As V_{g2} becomes more negative, the oscillation amplitude and the SDE decrease. Finally, when the supercurrent in JJ2 disappears for $V_{g2} \leq -1.8$ V as indicated in Fig. 1d, the SDE vanishes; when V_{g2} is even more negative, the oscillation disappears and the switching current of JJ1 with no coherent coupling remains. This demonstrates that the observed SDE is generated only when JJ2 is switched on and is therefore not attributable to any other mechanisms for SDE in single JJs[9] or to a possible vortex insertion in the SC electrodes[3,36]. The maximum $|I_{sw}|$ (in the $\phi_2 (\mathrm{mod}\, 2\pi) = 0$ neighbourhood, B in the range 0.01–0.168 mT) in the coupled case (V_{g2} = −1.4 V and −1.6 V) exceeds $|I_{sw}|$ in the single JJ1 case (V_{g2} = −2.0 V). This is one of the expected features as a consequence of the coherent coupling between JJ1 and JJ2. The coherent coupling of JJ1 and JJ2 is formed when penetration lengths of wavefunctions of the Andreev bound states are longer than the centre electrode thickness, as conceptually shown in Fig. 1a. When JJ2 is switched off, the partial wavefunctions of JJ1 penetrating JJ2 disappear and do not contribute to the supercurrent in JJ1. Therefore, the JJ1 switching current with JJ2 off is smaller than that when JJ2 is on at $\phi_2 = 0$.

Figure 3b shows $|I_{sw}|$ in JJ1 as a function of B at V_{g1} = −1.2 to −1.6 V with V_{g2} = 0 V, LJJ1 off and LJJ2 on, corresponding to the results with the local gate control of JJ1. As V_{g1} becomes more negative, both $|I_{sw+}|$ and $|I_{sw-}|$ decrease. The results indicate that a more negative V_{g1} decreases the SDE markedly. We define the SDE ratio as $\eta \equiv \frac{|I_{sw+}| - |I_{sw-}|}{|I_{sw+}| + |I_{sw-}|}$ and focus on B = 0.0768 mT, where the largest SDE for $|I_{sw+}| < |I_{sw-}|$ is obtained at V_{g2} = −1.4 V in Fig. 3a, highlighted by the black arrow. In this case, η = −0.064 at V_{g1} = −1.2 V, whereas η = −0.016 at V_{g1} = −1.6 V. Notably, a negative η is obtained for $|I_{sw+}| < |I_{sw-}|$ at B = 0.0768 mT; therefore, the larger SDE at B = 0.0768 mT is represented by the more negative η. This result reveals that the observed SDE does not originate from the asymmetric SQUID formed by JJ2 and LJJ2; if this was the case[12,14], η would not depend on the local gate voltage of JJ1, which is outside of the SQUID.

To clarify a relationship between the observed SDE and the correlation between JJ1 and JJ2, we fix B = 0.0768 mT and measure I_{sw+} and I_{sw-} as a function of V_{g1} and V_{g2}. Figure 3c shows $|I_{sw+}|$ and $|I_{sw-}|$ as functions of V_{g2} at V_{g1} = −1.25, −1.375 and −1.5 V, with LJJ1 off and LJJ2 on. At V_{g1} = −1.25 V and −1.375 V, the SDE decreases monotonically as V_{g2} decreases. On the other hand, the SDE at V_{g1} = −1.5 V becomes

the largest with $\eta = -0.075$ at $V_{g2} = -1.525$ V. Figure 3d shows the evaluated η as a function of V_{g1} and V_{g2} at $B = 0.0768$ mT. The blue region corresponding to the large SDE appears diagonally on the V_{g1}–V_{g2} graph; this diagonal SDE dependence seen in Fig. 3d indicates that η, corresponding to the SDE at $V_{g1} = -1.5$ V, nonmonotonically depends on V_{g2} in Fig. 3c. A grey curve in Fig. 3d indicates (V_{g1}, V_{g2}) combinations for which I_{sw} of the single JJ1 (with JJ2 off) at the V_{g1} is equal to I_{sw} of the single JJ2 (with JJ1 off) at the V_{g2}. Consequently, the blue SDE region follows the grey curve, indicating that the symmetric condition of JJ1 and JJ2 is significant for observing the SDE in our device. The mirrored structure device also indicates a similar gate dependence of the SDE with the sign reversed (Supplementary Note 3 and Supplementary Fig. 4). The coherent coupling of the two JJs is formed when the Andreev bound states in JJ1 and JJ2 hold the same energies. Thus, when the number of bound states, energies and transmissions of the JJs are similar or the same, the coherent coupling affects the supercurrent transport more markedly. Therefore, the symmetric condition of the JJs' switching current that produces a larger SDE in the experiments is reasonable for the SDE originating from the coherent coupling of the JJs. Further, the inductance effect cannot generate such gate dependence of η, because the SDE generated by the inductance and the bias current I_1 decreases monotonically as I_1 becomes smaller. Thus, if the SDE was produced by the inductance of the SC loop, only the local gate control would monotonically decrease the SDE; if that was the case, there would be no diagonal feature as shown in Fig. 3d (Supplementary Note 4 and Supplementary Figs. 5–6).

SDE origins

Theoretically, the coherent coupling of the Andreev bound states and the SDE are generated by two coexisting mechanisms: elastic cotunneling and crossed Andreev reflection[21]. Here, cotunneling implies quasiparticle tunnelling through the central SC electrode from JJ1 to JJ2, whereas the crossed Andreev reflection[37–39] describes the tunneling of an electron from JJ1 into JJ2 as a hole. Owing to the two mechanisms having the different coupling energies, the Andreev bound states' energies (as a function of ϕ_1 with a fixed $\phi_2 \neq 0, \pi$) become asymmetric to $\phi_1 = 0$, resulting in the asymmetric CPR of JJ1 because the supercurrent is proportional to the differential of the energies by ϕ_1 (ref. 21). This asymmetric CPR allows the difference between positive and negative switching currents, thus providing the SDE.

In the literature[21], the predicted CPR indicates a finite supercurrent at $\phi_1 = 0$ (namely, at the φ junction), in which the ground state of a JJ appears at a finite phase difference far from 0 or π (refs. 40–46). Thus, the obtained SDE can be an experimental signature of the φ junction formation in JJ1. The φ junction is expected to be applied to cryogenic memory cells[47] and phase batteries[48,49]. Our results can also be explained without considering the spin–orbit interactions present in InAs quantum wells. Recently, such spin–orbit interactions have been reported as playing an important role in the SDE observed in single JJs in the presence of an in-plane magnetic field[9]. The in-plane magnetic field may be utilized to study the physics of the spin–orbit interactions in the SDE in the coupled JJs. Further experimental studies to reveal the φ junction and the spin–orbit interaction roles in the SDE are required to establish the coupled JJ physics and to evaluate any potential applications.

To establish the physics of these coupled JJs, the Andreev spectrum must be observed; this will be accomplished by tunnel spectroscopy of the respective JJs, as reported previously for multiterminal JJs[50].

Conclusion

In conclusion, we demonstrate that the SDE in a JJ controlled by the non-local phase difference emerges from the coherent coupling of two JJs. The local and non-local gate-voltage dependencies indicate that the SDE is greatest when the two JJs become nearly equivalent, implying that the observed SDE is derived from the coherent coupling between two JJs. The SDE observations indicate that there are two different coupling mechanisms, elastic cotunneling and crossed Andreev reflection, possessing different coupling energies. Our results indicate that the time-reversal and spatial-inversion symmetries in one JJ are broken by non-local control of the other coupled JJ. This means that the coupled JJs will be platforms to exploit the exotic SC phenomena, which have been demonstrated with the SC systems of the spin–orbit interactions and the strong magnetic fields and are available to design SC diode devices in SC circuits.

Online content

Any methods, additional references, Nature Portfolio reporting summaries, source data, extended data, supplementary information, acknowledgements, peer review information; details of author contributions and competing interests; and statements of data and code availability are available at https://doi.org/10.1038/s41567-023-02144-x.

References

1. Lutchyn, R. M. et al. Majorana zero modes in superconductor–semiconductor heterostructures. *Nat. Rev. Mater.* **3**, 52–68 (2018).
2. Raissi, F. & Nordman, J. E. Josephson fluxonic diode. *Appl. Phys. Lett.* **65**, 1838–1840 (1994).
3. Carapella, G. & Costabile, G. Ratchet effect: demonstration of a relativistic fluxon diode. *Phys. Rev. Lett.* **87**, 077002 (2001).
4. Beck, M. et al. High-efficiency deterministic Jjosephson vortex ratchet. *Phys. Rev. Lett.* **95**, 090603 (2005).
5. Sterck, A., Kleiner, R. & Koelle, D. Three-junction SQUID rocking ratchet. *Phys. Rev. Lett.* **95**, 177006 (2005).
6. Sterck, A., Koelle, D. & Kleiner, R. Rectification in a stochastically driven three-junction SQUID rocking ratchet. *Phys. Rev. Lett.* **103**, 047001 (2009).
7. Sickinger, H. et al. Experimental evidence of a φ Josephson junction. *Phys. Rev. Lett.* **109**, 107002 (2012).
8. Menditto, R. et al. Tunable φ Josephson junction ratchet. *Phys. Rev. E* **94**, 042202 (2016).
9. Baumgartner, C. et al. Supercurrent rectification and magnetochiral effects in symmetric Josephson junctions. *Nat. Nanotechnol.* **17**, 39–44 (2022).
10. Turini, B. et al. Josephson diode effect in high-mobility InSb nanoflags. *Nano Lett.* **22**, 8502–8508 (2022).
11. Pal, B. et al. Josephson diode effect from Cooper pair momentum in a topological semimetal. *Nat. Phys.* **18**, 1228–1233 (2022).
12. Thompson, M. D. et al. Graphene-based tunable SQUIDs. *Appl. Phys. Lett.* **110**, 162602 (2017).
13. Murphy, A. & Bezryadin, A. Asymmetric nanowire SQUID: linear current-phase relation, stochastic switching, and symmetries. *Phys. Rev. B* **96**, 094507 (2017).
14. Souto, R. S., Leijnse, M. & Schrade, C. The Josephson diode effect in supercurrent interferometers. *Phys. Rev. Lett.* **129**, 267702 (2022).
15. Wakatsuki, R. et al. Nonreciprocal charge transport in noncentrosymmetric superconductors. *Sci. Adv.* **3**, e1602390 (2017).
16. Qin, F. et al. Superconductivity in a chiral nanotube. *Nat. Commun.* **8**, 14465 (2017).
17. Ando, F. et al. Observation of superconducting diode effect. *Nature* **584**, 373–376 (2020).
18. Miyasaka, Y. et al. Observation of nonreciprocal superconducting critical field. *Appl. Phys. Express* **14**, 073003 (2021).
19. Diez-Merida, J. et al. Symmetry-broken Josephson junctions and superconducting diodes in magic-angle twisted bilayer graphene. *Nat. Commun.* **14**, 2396 (2023).
20. Lin, J.-X. et al. Zero-field superconducting diode effect in small-twist-angle trilayer graphene. *Nat. Phys.* **18**, 1221–1227 (2022).

21. Pillet, J.-D., Benzoni, V., Griesmar, J., Smirr, J.-L. & Girit, Ç. Ö. Nonlocal Josephson effect in Andreev molecules. *Nano Lett.* **19**, 7138–7143 (2019).
22. Kornich, V., Barakov, H. S. & Nazarov, Y. V. Fine energy splitting of overlapping Andreev bound states in multiterminal superconducting nanostructures. *Phys. Rev. Res.* **1**, 033004 (2019).
23. Kornich, V., Barakov, H. S. & Nazarov, Y. V. Overlapping Andreev states in semiconducting nanowires: competition of one-dimensional and three-dimensional propagation. *Phys. Rev. B* **101**, 195430 (2020).
24. Matsuo, S. et al. Observation of nonlocal Josephson effect on double InAs nanowires. *Commun. Phys.* **5**, 221 (2022).
25. Sau, J. D. & Sarma, S. D. Realizing a robust practical Majorana chain in a quantum-dot-superconductor linear array. *Nat. Commun.* **3**, 1966 (2012).
26. Draelos, A. W. et al. Supercurrent flow in multiterminal graphene Josephson junctions. *Nano Lett.* **19**, 1039–1043 (2019).
27. Pankratova, N. et al. Multiterminal Josephson effect. *Phys. Rev. X* **10**, 031051 (2020).
28. Graziano, G. V., Lee, J. S., Pendharkar, M., Palmstrøm, C. J. & Pribiag, V. S. Transport studies in a gate-tunable three-terminal Josephson junction. *Phys. Rev. B* **101**, 054510 (2020).
29. Arnault, E. G. et al. Dynamical stabilization of multiplet supercurrents in multiterminal Josephson junctions. *Nano Lett.* **22**, 7073–7079 (2022).
30. Chiles, J. et al. Nonreciprocal supercurrents in a field-free graphene Josephson triode. *Nano Lett.* **23**, 5257–5263 (2023).
31. Zhang, F. et al. Andreev processes in mesoscopic multi-terminal graphene Josephson junctions. *Phys. Rev. B* **107**, L140503 (2023).
32. Gupta, M. et al. Superconducting diode effect in a three-terminal Josephson device. *Nat. Commun.* **14**, 3078 (2023).
33. Nichele, F. et al. Scaling of Majorana zero-bias conductance peaks. *Phys. Rev. Lett.* **119**, 136803 (2017).
34. Kjaergaard, M. et al. Quantized conductance doubling and hard gap in a two-dimensional semiconductor-superconductor heterostructure. *Nat. Commun.* **7**, 12841 (2016).
35. Kjaergaard, M. et al. Transparent semiconductor-superconductor interface and induced gap in an epitaxial heterostructure Josephson junction. *Phys. Rev. Appl.* **7**, 034029 (2017).
36. Golod, T. & Krasnov, V. M. Demonstration of a superconducting diode-with-memory, operational at zero magnetic field with switchable nonreciprocity. *Nat. Commun.* **13**, 3658 (2022).
37. den Hartog, S. G., Kapteyn, C. M. A., van Wees, B. J., Klapwijk, T. M. & Borghs, G. Transport in multiterminal normal-superconductor devices: reciprocity relations, negative and nonlocal resistances, and reentrance of the proximity effect. *Phys. Rev. Lett.* **77**, 4954 (1996).
38. Mélin, R. & Feinberg, D. Sign of the crossed conductances at a ferromagnet/superconductor/ferromagnet double interface. *Phys. Rev. B* **70**, 174509 (2004).
39. Russo, S., Kroug, M., Klapwijk, T. M. & Morpurgo, A. F. Experimental observation of bias-dependent nonlocal Andreev reflection. *Phys. Rev. Lett.* **95**, 027002 (2005).
40. Buzdin, A. & Koshelev, A. E. Periodic alternating 0- and π-junction structures as realization of φ-Josephson junctions. *Phys. Rev. B* **67**, 220504 (2003).
41. Buzdin, A. Direct coupling between magnetism and superconducting current in the Josephson φ_0 junction. *Phys. Rev. Lett.* **101**, 107005 (2008).
42. Tanaka, Y., Yokoyama, T. & Nagaosa, N. Manipulation of the Majorana fermion, Andreev reflection, and Josephson current on topological insulators. *Phys. Rev. Lett.* **103**, 107002 (2009).
43. Reynoso, A. A., Usaj, G., Balseiro, C. A., Feinberg, D. & Avignon, M. Anomalous Josephson current in junctions with spin polarizing quantum point contacts. *Phys. Rev. Lett.* **101**, 107001 (2008).
44. Yokoyama, T., Eto, M. & Nazarov, Y. V. Anomalous Josephson effect induced by spin-orbit interaction and Zeeman effect in semiconductor nanowires. *Phys. Rev. B* **89**, 195407 (2014).
45. Szombati, D. B. et al. Josephson ϕ_0-junction in nanowire quantum dots. *Nat. Phys.* **12**, 568–572 (2016).
46. Mayer, W. et al. Gate controlled anomalous phase shift in Al/InAs Josephson junctions. *Nat. Commun.* **11**, 212 (2020).
47. Goldobin, E. et al. Memory cell based on a φ Josephson junction. *Appl. Phys. Lett.* **102**, 242602 (2013).
48. Pal, S. & Benjamin, C. Quantized Josephson phase battery. *EPL (Europhys. Lett.)* **126**, 57002 (2019).
49. Strambini, E. et al. A Josephson phase battery. *Nat. Nanotechnol.* **15**, 656–660 (2020).
50. Strambini, E. et al. The ω-SQUIPT as a tool to phase-engineer Josephson topological materials. *Nat. Nanotechnol.* **11**, 1055–1059 (2016).

Methods

Sample growth

The wafer structure was grown via molecular beam epitaxy on a semi-insulating InP substrate. The stack materials from bottom to top are a 100 nm $In_{0.52}Al_{0.48}As$ buffer, a 5 period 2.5 nm $In_{0.53}Ga_{0.47}As$/2.5 nm $In_{0.52}Al_{0.48}As$ superlattice, a 1-µm-thick metamorphic graded buffer stepped from $In_{0.52}Al_{0.48}As$ to $In_{0.84}Al_{0.16}As$, a 33 nm graded $In_{0.84}Al_{0.16}As$ to $In_{0.81}Al_{0.19}As$ layer, a 25 nm $In_{0.81}Al_{0.19}As$ layer, a 4 nm $In_{0.81}Ga_{0.19}As$ lower barrier, a 5 nm InAs quantum well, a 10 nm $In_{0.81}Ga_{0.19}As$ top barrier, two monolayers of GaAs and finally an 8.7 nm layer of epitaxial Al. The top Al layer has been grown in the same chamber without breaking the vacuum. The two-dimensional electron gas accumulates in the InAs quantum well.

Device fabrication

The JJs were fabricated using conventional electron beam lithography with polymethyl methacrylate. The aluminium film was etched out using a type-D etchant after defining the mesa of the InAs quantum well with a 1:1:8 H_3PO_4, H_2O_2 and H_2O etchant ratio. Then, a 30-nm-thick Al_2O_3 film was grown by atomic layer deposition and Ti and Au were deposited to obtain the gate electrodes.

Data availability

The data that support the findings of this study are available from the Zenodo repository at https://doi.org/10.5281/zenodo.8024898. Source data are provided with this paper.

Acknowledgements

S.M. and S.T. acknowledge a JSPS Grant-in-Aid for Scientific Research (S) (Grant No. JP19H05610). S.M. acknowledges JST PRESTO (Grant No. JPMJPR18L8), JST FOREST (Grant No. JPMJFR223A), Advanced Technology Institute Research Grants and the Ozawa-Yoshikawa Memorial Electronics Research Foundation. T.Y. acknowledges JSPS Grant-in-Aid for Early-Career Scientists (Grant No. 18K13484).

Author contributions

S.M. designed the experiments. T.L., S.G., G.C.G., and M.J.M. grew wafers to form InAs 2DEG quantum wells covered with epitaxial aluminium. S.M. fabricated the devices. S.M. and T.I. performed measurements. S.M., T.I., Y.S. and S.T. analysed the data. T.Y. performed numerical calculations. S.T. supervised the study.

Competing interests

The authors declare no competing interests.

Additional information

Supplementary information The online version contains supplementary material available at https://doi.org/10.1038/s41567-023-02144-x.

Correspondence and requests for materials should be addressed to Sadashige Matsuo or Seigo Tarucha.

Peer review information *Nature Physics* thanks Morteza Kayyalha and the other, anonymous, reviewer(s) for their contribution to the peer review of this work.